THE POWER SPECTRUM OF COSMIC MICROWAVE BACKGROUND POLARIZATION FROM COSMIC STRING WAKES

GRANT SALTON

Master of Science
Department of Physics
McGill University

A thesis submitted to McGill University in partial fulfillment of the requirements of the degree of Master of Science.

December 13, 2013

Careful. We don't want to learn from this.

— Bill Watterson, "*Calvin and Hobbes*"

For Ginny.

ACKNOWLEDGEMENTS

Summarizing everyone who influenced me in one form or another is a daunting task. There are, of course, those people who deserve special praise – more than should be offered in the acknowledgement section of a thesis. Nonetheless, I shall mention these commendable individuals in the absence of tangible reward.

Firstly, I'd like to thank my supervisors, professors Robert Brandenberger and Patrick Hayden, for their guidance and wisdom over the last two years. Professor Brandenberger proposed the project which eventually became this thesis and was instrumental in preparation of this document. I am extremely grateful for his academic support and personal advice; he is an excellent *supervisor* of students. I would also like to thank Professor Hayden for allowing me to write my thesis on a topic unrelated to his own research. As an interdisciplinary student, I value the intellectual stimulation and anchoring professor Hayden provided, and I aspire (in vain) to be a researcher of his calibre.

My parents, who supported my decisions and aspirations from a young age, also supported me financially for many years. I thank them for overlooking my foibles and the unhealthy lifestyle of an undergraduate physics student, and for supporting me nonetheless. They also helped with proofreading of this document. My sister, Leanne, deserves mention though not for doing anything.

What is a physics degree without the unfortunate souls who share the experience? My friends and office mates made my time at McGill a pleasure. In a very particular (alphabetical) order they are: Adam Bognat, Alex "Basakyat" Belin, Ediot Kuhano, Frank Duplessis, Jöel Beaudry, Kuhan "The Kuhan" Wang, Mohammed Harb, Philippe Giguère, Samwise Selgamgee, and Yuuki Omori. Special thanks to Phil and Frank for help with French translation.

I would like to mention my collaborator and friend, Nick Menicucci, for teaching me valuble research lessons and for perservering through a seemingly endless integral. He unknowingly served as a mentor for many years. As well, I thank my friend Matt Bamsey for continuing to be an inspiration to me.

Ginny Phixaykoune, my best friend and wonderful girlfriend, has supported me through everything a physics degree has to offer. Through thick and thin she selflessly exercised enormous understanding, and for this I am truly grateful. A life–long companion, Ginny always took interest in my studies and offered her assistance whenever possible. She too is an inspiration, and she deserves extra credit for proofreading.

Thank you all.

ABSTRACT

We compute the integrated Sachs–Wolfe type contribution to the CMB polarization power spectrum from cosmic string wakes. An introduction to topological defects, cosmic strings, CMB polarization, and spin–s fields is given. We then use these tools to compute the angular power spectrum of E– and B–mode polarization due to cosmic string wakes, in the flat sky limit. We find that cross–correlation terms (i.e., EB, ET, BT) vanish, while the EE and BB power spectra are equal in shape and magnitude. This result is in stark contrast with B–mode polarization from Gaussian fluctuations, which vanishes identically. However, we find that the shape of the power spectrum from cosmic string wakes is very similar to the predicted B–mode power spectrum from gravitational lensing, but with a small overall amplitude. As such, the cosmic string wake signal is too small to be picked out from lensing, and background subtraction techniques would be very difficult. We find that the peak amplitude in the dimensionless power spectrum ($\sqrt{l(l+1)C_l/2\pi}$) is about 10^{-4} at a peak value of $l \sim 400$.

We briefly study the asymptotic version of the power spectrum and find that C_l is approximately constant until a turn around point set by the angular size of the dominant wakes. We then determine which cosmic string wakes give rise to the dominant contribution to the full, integrated power spectrum and find that the dominant wakes are those which were formed at the time of equal matter and radiation, and which intersect our past light cone at recombination. We conclude that the Fourier space signal (power spectrum) is too weak to detect cosmic string wakes in existing data, and future searches should focus on distinct position space features.

ABRÉGÉ

Nous calculons la contribution intégrée au spectre de puissance de la polarisation du fond diffus cosmique (CMB) grâce aux sillages des cordes cosmiques. Une introduction aux défauts topologique, cordes cosmiques, de polarisation du CMB, et aux champs spin–s est donnée. Nous utilisons ensuite ces outils pour calculer le spectre de puissance angulaire de la polarisation des modes E et B grâce aux des sillages des cordes cosmiques, dans la limite du ciel plat. Nous trouvons que les termes de corrélation croisée (EB, ET, BT) sont zero, tandis que les spectres de puissance pour EE et BB ont la même forme et grandeur. Ce résultat contraste le polarisation du mode B causée par les fluctuations Gaussiennes, qui disparaîssent. Cependant, nous trouvons que la forme du spectre de puissance causée par les sillages de cordes cosmiques est très similaire au spectre en mode B prédite par lentille gravitationnelle, mais avec une amplitude globale trés faible. Donc, le signal du sillage de corde cosmique est trop faible pour être measuré au-dessus l'indicatif du lentille. Aussi, les méthodes de soustraction du fond serait très difficile. Nous trouvons que l'amplitude maximum dans le spectre de puissance ($\sqrt{l(l+1)C_l/2\pi}$) est d'environ 10^{-4} pour $l \sim 400$.

Nous étudions brièvement le forme asymptotique du spectre de puissance, et nous trouvons que C_l est quasi–constant en l jusqu'à un tournant correspondant à la taille angulaire du sillage le plus important. Nous déterminons alors quel sillage donne la contribution dominante au spectre de puissance complet. Nous trouvons que les sillages dominants sont ceux qui ont été formés à l'epoque de l'égalité de matière et de rayonnement, et qui croisent notre cône de lumière passé à l'époque de recombinaison. Nous concluons que l'indicatif dans l'espace Fourier est trop faible pour être détecté. Donc, les recherches futures devraient se concentrer sur les caractéristiques l'espace spatial.

CONTENTS

LIST OF FIGURES

1

INTRODUCTION

Topological defects are decidedly underrepresented in physics. They arise whenever a system undergoes a phase of symmetry breaking and are natural and robust phenomena. Most physicists first gain familiarity with topological defects in the context of domain walls separating two regions with oppositely aligned spins in magnets, yet few realize their importance in other areas of physics. Topological defects form during symmetry breaking phase transitions. Perhaps the best known example of spontaneous symmetry breaking is the process which gives rise to the recently discovered Higgs boson [1]. Other well known examples (relating to superconductivity and superfluidity) arise in condensed matter systems and have been well studied [2]. We will discuss this type of symmetry breaking in section 1.1, with a cosmological application in mind. Note that, although topological defects have been seen in a number of systems, we have not yet observed them in field theory models. While one can consider cosmological domain walls, they would tend to dominate the energy density of the universe, and are therefore problematic and have been ruled out by observation [3]. Instead, we will consider one dimensional, filamentary defects known as cosmic strings. Cosmic strings are topological defects formed during the symmetry breaking (e.g., electroweak symmetry breaking) phases of our universe through finite temperature effects. Physically, they are regions of

trapped potential energy which interact gravitationally with observable matter. Since they form in the early universe and interact with their surroundings, they could give rise to observable signatures (see [4, 5] for a review). Many of these signatures have been studied in a great deal of detail, which has allowed us to place upper bounds on the physical parameters characterizing cosmic strings [6, 7, 8, 9, 10, 11, 12, 13, 14]. An example of an emerging observational window with no shortage of cosmic string literature is 21cm radiation [15, 16, 17]. However, a particularly promising observational window in which to look for cosmic strings is that of cosmic microwave background (CMB) polarization. In particular, we will focus our efforts on B–mode polarization, which is a particular pattern in the CMB polarization vector field. B–mode polarization is suggested to be the cleanest detection mode for cosmic-strings, rather than the related E–mode polarization or standard temperature anisotropies. Recent advancements in polarization telescopes are pushing observations closer to the precision measurement of B–mode polarization (e.g., [18, 19]). In fact, the South Pole Telescope recently announced the first detection of B–mode polarization [20]. When a cosmic string moves through spacetime, it leaves behind it a wake of overdensity in the background matter field. As such these wakes would produce cold spots in the CMB with characteristic position space features. Danos et al. [21] found that the signature of cosmic string wakes corresponds to a roughly rectangular patch on the sky with a linear fade in the polarization strength along one axis of the rectangle. Our aim is to study the overall effect of a network of cosmic string wakes on the observed CMB polarization.

1.1 TOPOLOGICAL DEFECTS AND COSMIC STRINGS

This section is based on the book by Vilenkin and Shellard [22] and serves as a lightning introduction to cosmic strings. Topological defects are an extremely rich and fruitful subject, and an in depth analysis is not necessary for our purposes. Instead, we will focus on a specific class of topological defects known as strings, and in particular those formed by second–order phase transitions. For those familiar with the subject, we will not concern ourselves with the vacuum manifold, homotopy groups, or any other such beasts. Rather, we will employ an intuitive picture and refer interested readers to Vilenkin and Shellard [22] for details. Furthermore, it will prove useful to begin our study of topological defects with *domain walls*, as they are easier to conceptualize, they form from a simpler Lagrangian, and they help build intuition.

The starting point for domain walls of the kind we want is a ϕ^4 scalar field with a temperature dependent mass. In particular, we have a temperature dependent Lagrangian of the form

$$\mathcal{L} = \frac{1}{2}\partial_\mu\bar{\phi}\partial^\mu\phi - V_{\text{eff}}(|\phi|) \tag{1.1}$$

$$V_{\text{eff}}(|\phi|) = m^2(T)|\phi|^2 + \frac{\lambda}{4}|\phi|^4, \tag{1.2}$$

where m is the mass of the scalar field, λ is a coupling constant, T is the temperature of the field, and we can assume $\phi \in \mathbb{R}$ WLOG. In order to get a spontaneous symmetry breaking potential, the temperature dependent mass takes the form

$$m^2(T) = \frac{\lambda}{12}(T^2 - 6\eta^2), \tag{1.3}$$

where η is the *vev* (vacuum expectation value) of the field after symmetry breaking. It is clear from the form of $m^2(T)$ that there is a critical tempera-

ture, $T_C = \sqrt{6}\eta$, at which $m = 0$. This effective potential has the property

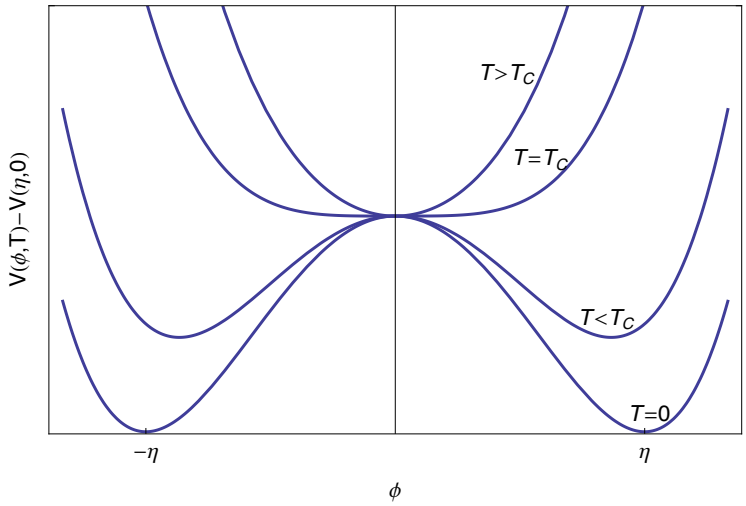

Figure 1: A spontaneous symmetry breaking potential. For large T, the field is in a stable configuration around $\phi = 0$. However, as the temperature decreases beyond the stable, critical temperature T_C, the potential takes on the familiar double well (Mexican hat) shape. When this occurs, the field acquires a *vev*, and different regions of space will have the field break to one of the two degenerate vacua ($\phi = \pm\eta$)

that it gives rise to a stable minimum at $\phi = 0$ for temperatures greater than T_C, and corresponds to an unstable vacuum at $\phi = 0$ for $T < T_C$. Figure 1 shows the shape of V_{eff} for different values of T. For large temperatures, this corresponds to a homogeneous field in the ground state $\phi = 0$ (up to local quantum fluctuations) everywhere in space. As the universe cools, the temperature eventually dips below the critical temperature, causing ϕ to attain a non–zero *vev*. Since local quantum fluctuations tend to bias the field to one side of the unstable point at $\phi = 0$, different regions in space will have the field transition to different minima ($\phi = \pm\eta$). When this happens, spatial continuity of the quantum field requires that there be a region in space in which the value of the field changes from $\phi = -\eta$ to $\phi = +\eta$. The halfway point of this region would therefore have $\phi = 0$, as illustrated in fig. 2. However, $V_{\text{eff}}(\phi = 0, T < T_C)$ does not correspond to the ground state, and it is in this sense that we say the topological defect (domain wall) corresponds to a region

of trapped potential energy. Extending this argument into additional spatial dimensions leaves us with a two–dimensional planar topological defect – the domain wall.

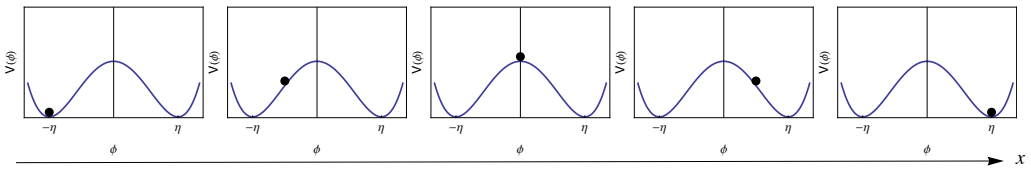

Figure 2: Formation of topological defects as a consequence of spatial continuity of quantum fields. During the second order phase transition shown in fig. 1, regions of space may break to different values of the new degenerate ground state. However, continuity of the field in space demands a region between two different vacua in which $\phi(x)$ is not in the ground state. In this figure, the horizontal direction is space, and we are illustrating the field configuration as a function of position.

We now build on the intuition gained from domain walls to study the formation of cosmic strings. Consider the simple gauge theory describing scalar electrodynamics (also known as the abelian–Higgs model), which consists of a *complex* (or otherwise multi-component) scalar field ϕ and a gauge field A_μ. The Lagrangian density for this theory is given by

$$\mathcal{L} = \frac{1}{2}\mathcal{D}_\mu\bar{\phi}\mathcal{D}^\mu\phi - V(\phi) - \frac{1}{4}F_{\mu\nu}F^{\mu\nu}, \tag{1.4}$$

where $\mathcal{D}_\mu = \partial_\mu - ieA_\mu$ is the gauge covariant derivative, e is the gauge coupling, and $F_{\mu\nu} = \partial_\mu A_\nu - \partial_\nu A_\mu$ is the field strength tensor. The potential, $V(\phi)$ is similar to eq. (1.2) for low temperatures, and is given by

$$V(\phi) = \frac{1}{4}\lambda(\bar{\phi}\phi - \eta^2)^2, \tag{1.5}$$

where λ is a coupling constant, and η corresponds to the *vev* as before. The potential is shown in fig. 3. Note that this theory admits a local $U(1)$ symmetry, which is spontaneously broken when ϕ attains a *vev* ($|\phi| = \eta$).

Varying the action and solving for the equations of motion, one finds that there exist solitonic solutions, which are translationally invariant along one direction of space. Choosing this invariant direction to be z and constructing cylindrical coordinates for the global space, we can fix a slice in z and work in polar coordinates (r, θ) for the other two directions. These translationally invariant string configurations are given by

$$\phi(r, \theta) = \eta e^{i\theta} \tag{1.6}$$

for large r. This field configuration has the curious property that there must exist a point at which $\phi = 0$ to avoid an undefined phase (see fig. 4a). The presence of this non–vacuum point is a consequence of continuity: since the phase in eq. (1.6) at some radius r changes from 0 to 2π as we traverse a circle in position space, the phase of ϕ at the center of this circle must change from 0 through 2π at a single point. The only way to resolve this ill–defined field value is if $\phi = 0$ at this point. Since $V(\phi = 0) \neq 0$, we say that the cosmic string is a region of trapped potential energy.

Recall that the field configuration in eq. (1.6) is translationally invariant along the z direction. As such, we can freely extend the above analysis along

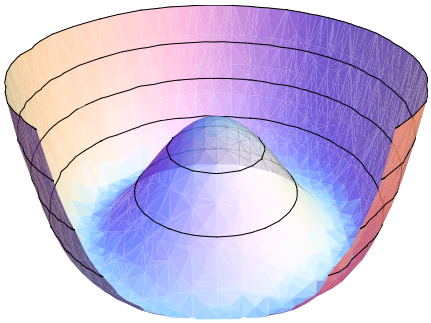

Figure 3: The symmetry breaking potential for the abelian–Higgs model. The potential has the familiar "Mexican hat" shape, with an unstable local maximum at $\phi = 0$. The field undergoes spontaneous symmetry breaking and ϕ obtains a *vev* at $V = 0$ with $|\phi| = \eta$.

z to finally arrive at a long, filamentary topological defect – the cosmic string. This spatial extension is shown in fig. 4b.

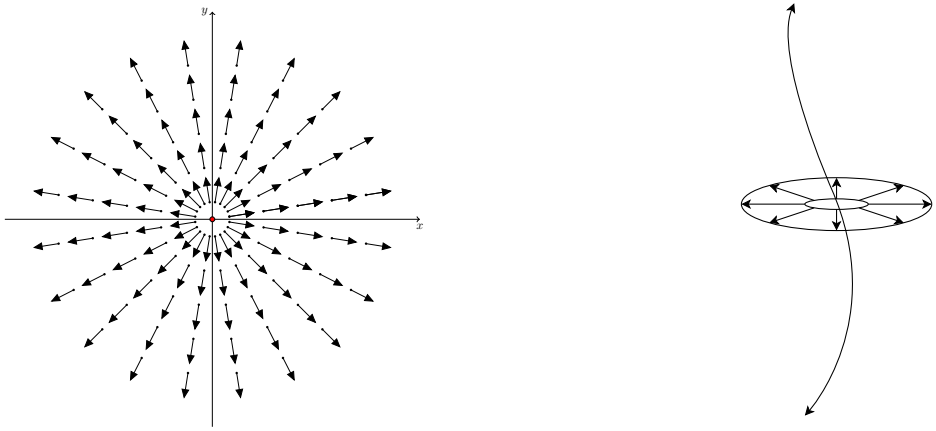

(a) Winding in the field configuration causes an ill–defined phase at the origin.

(b) Translation invariance along one direction forms the one–dimensional string structure.

Figure 4: Formation of a cosmic string due to non–trivial winding in the field configuration. The cosmic string field configuration given in eq. (1.6) has the property that the phase of ϕ is undefined at $r = 0$. In order to reconcile this fact, continuity of the quantum field dictates that ϕ must be zero at this point. Since the field configuration is translationally invariant along the z direction, we extend the analysis along z and find that there must be a one dimensional line of trapped potential energy.

One possible argument against the field configuration in eq. (1.6) is that it may not be physically realizable. There are many valid field configurations which solve the equations of motion, but they may not be relevant for any physical theory. However, a very simple argument due to Kibble [23] shows that these cosmic string configurations are not only physically relevant, but are robust and arise naturally. The argument is based on causality and proceeds as follows. Suppose we have a theory which admits topological defect solutions, say eq. (1.4) with eq. (1.6). Since correlations in the state of the field cannot persist over length scales larger than the horizon length, the phase of ϕ should appear randomly distributed on super–horizon scales. As such, we will inevitably form cosmic string states with a non–trivial winding in the phase of

ϕ, which gives rise to topological defects. In the context of domain walls, the Kibble mechanism says that the field ϕ should break to different degenerate vacua on scales larger than the horizon scale. As such, topological defect solutions should arise on physical grounds, and we expect cosmic strings to form during any symmetry breaking transition in our universe. It is important to note, however, that many observational searches for cosmic strings have been conducted, without providing evidence for their existence.

In addition to (infinitely) long strings, another stable topological defect is a loop. Imagine joining two ends of a long string together to form a loop such that the interior and exterior have different ground states. Such an object constitutes a valid field configuration and provides additional features one can study. However, cosmic string loops will tend to oscillate and wiggle due to their string tension. This motion induces fluctuations in the gravitational field and the loop radiates gravitational waves. As such, the energy in the loop decreases and the loops eventually decay [5]. Thus, we will henceforth focus our efforts on long strings, rather than cosmic string loops.

1.2 COSMIC STRING WAKES

When cosmic strings move in a direction normal to their length with relativistic speeds, they create a wake in their path. The requirement that strings move at relativistic speeds comes from the nature of the dynamical equations. Since the wake equation we will solve below is relativistic, the only characteristic velocity in the problem is the speed of light. Wake creation is a relativistic effect and corresponds to the formation of a deficit angle in the geometry behind the wake. To see how this comes about, we consider a long, straight string lying static along the z–axis and calculate the metric. Since we wish to find the small

geometric effect of a cosmic string on the background spacetime, we work in the weak–field limit and let the metric $g_{\mu\nu}$ take the form

$$g_{\mu\nu} = \eta_{\mu\nu} + h_{\mu\nu}, \tag{1.7}$$

where $\eta_{\mu\nu}$ is the Minkowskian metric and $h_{\mu\nu}$ is the metric perturbation, subject to $|h_{\mu\nu}| \ll 1$. One can then show [22] (by fixing the harmonic gauge $\partial_\nu(h^\nu_\mu - \frac{1}{2}\delta^\nu_\mu h^\sigma_\sigma) = 0$) that the equations of motion for the metric perturbation are given by

$$\Box h_{\mu\nu} = -16\pi G\left(T_{\mu\nu} - \frac{1}{2}\eta_{\mu\nu}T^\sigma_\sigma\right). \tag{1.8}$$

For a stationary object lying along the z–direction, the mass–energy is localized in z and the energy–momentum tensor takes the form

$$T^\nu_\mu = \mu\delta(x)\delta(y)\mathrm{diag}(1,0,0,1), \tag{1.9}$$

where μ is the mass per unit length of the string. With this simplified energy–momentum tensor one can then rewrite the metric in spherical coordinates as

$$ds^2 = dt^2 - dz^2 - (1-h)(dr^2 + r^2 d\theta^2), \tag{1.10}$$

where $r = \sqrt{x^2+y^2}$, θ is the angular coordinate, and $h = 8G\mu\ln(r) - h_0$ with h_0 being a constant of integration. Defining new variables r' and θ' via

$$(1-8G\mu)r'^2 = (1-h)r^2 \tag{1.11}$$

$$\theta' = (1-4G\mu)\theta \tag{1.12}$$

and expanding the metric to leading order in $G\mu$, one obtains the result

$$ds^2 = dt^2 - dz^2 - dr'^2 - r'^2 d\theta'^2. \tag{1.13}$$

Thus, we see that the space near the cosmic string looks locally flat. This result is surprising at first because we expect the trapped potential energy in the string to have gravitational effects. So how, then, do cosmic strings interact and what are these all important wakes? Notice that the definition of θ' shifts the allowed range of the angular coordinate away from $[0, 2\pi)$. Instead, $\theta' \in [0, 2\pi(1 - 4G\mu))$ and we see that the space behind the string has a deficit angle compared to the space in front of the string. So while the space near a cosmic string appears locally flat, it is not *globally* flat. There is an azimuthal deficit angle

$$\Delta = 8\pi G\mu \tag{1.14}$$

corresponding to a wedge of spacetime which has been effectively carved out by the string with the exposed ends being glued together. Figure 5 shows a top

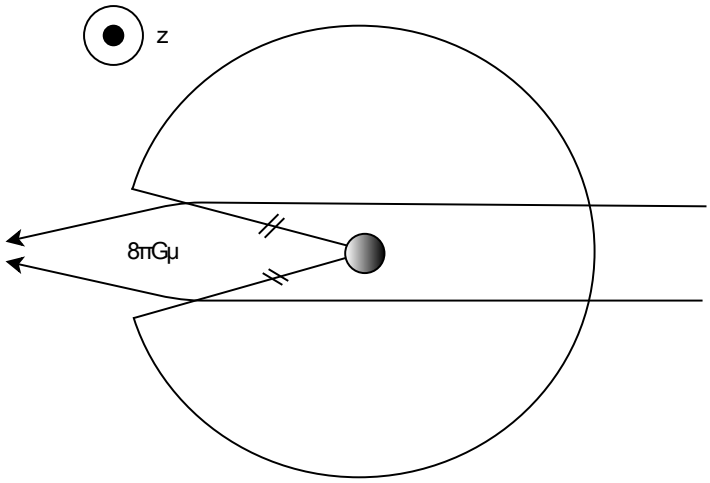

Figure 5: The formation of a cosmic string wake. In the rest frame of the cosmic string (here shown oriented along the z–axis), the region to the left of the string has a deficit angle and an associated conical geometry. Matter moving past the string appears deflected inward as it passes the cosmic string leaving a local overdensity.

down view of the formation of a deficit angle in the region behind the string. The figure is drawn in the rest frame of the cosmic string, and the exposed edges of the wedge behind the string have been identified. In the string frame, matter moving past the string appears to be deflected toward the plane behind the cosmic string as it enters the region with conical geometry. Since, at a given distance away from the string, there are two streams of matter particles (one on each side) which appear to be bent toward one another, it appears as though the area behind the string has an overdensity of matter relative to regions far away. In the rest frame of the matter the string passes by at relativistic speeds and the matter field experiences a kick toward the plane swept out by the string. This kick is felt by particles on the other side of the string, and the particles are perturbed toward one another into a region of local overdensity. The net result is a region of overdensity caused by the formation of a deficit angle in the spacetime geometry by cosmic strings moving at relativistic speeds, and is referred to as a *cosmic string wake*.

Once formed, wakes grow via gravitational accretion of additional matter. Since they correspond to regions of local overdensity containing free electrons, and because they have a distinct position space signal, cosmic string wakes present themselves as candidate sources for observable CMB polarization signals.

1.3 CMB POLARIZATION

Photon scattering from charged particles is a well studied phenomenon and has been thoroughly characterized in both the low and high energy regimes. For high energies, the scattering is inelastic and the process is known as Compton scattering. For lower energies, the scattering is well approximated as an

inelastic process and is known as Thomson scattering after J.J. Thomson. Polarization of photons in the CMB takes place at energies corresponding to Thomson scattering. For an excellent introduction to CMB polarization, the reader is referred to Hu and White [24].

It can be shown that the differential cross section for Thomson scattering is given by

$$\frac{d\sigma}{d\Omega} = \frac{3\sigma_T}{8\pi}|\hat{\boldsymbol{\epsilon}} \cdot \hat{\boldsymbol{\epsilon}}'|^2, \tag{1.15}$$

where $\hat{\boldsymbol{\epsilon}}$ and $\hat{\boldsymbol{\epsilon}}'$ are the incident and scattered photon polarization directions, respectively [25, 26]. We see from eq. (1.15) that the cross section is maximized when the incident and scattered radiation are parallel. Since we want the radiation to be scattered toward the observer (so that it can be observed!), and since Maxwell's equations require polarization to be perpendicular to the direction of travel, Thomson scattering provides a means for polarization. If the incident radiation field has an overall quadrupole moment, the resulting scattered photons will be polarized. Figure 6 shows an example of polarization due to Thomson scattering. If the CMB has an overall quadrupole moment relative to a free electron, radiation from Thomson scattering off this free electron will be polarized. Schematically, this appears to the observer as polarized light coming from a region in the CMB centered between two antipodal hot spots and two antipodal cold spots. This hot–cold pattern constitutes the required quadrupole and the observed light has been scattered by free electrons.

When presented with a polarization map or light intensity field, it is often convenient to use the Stokes parameters, Q, U, V, and I to describe polarized light (see [27] for a review.) The Stokes parameters are defined in terms of the x and y components of the electric field and relate to the intensity of light in different directions. To avoid unnecessary detail, we will paint a naive picture by aligning a compass rose with the page such that north points toward the

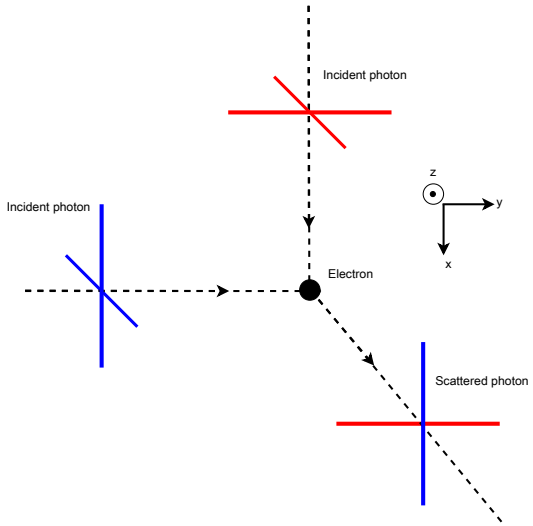

Figure 6: Polarization due to Thomson scattering. Light incident along the x (red) and y (blue) directions is polarized along the (y, z) and (x, z) directions, respectively. Thomson scattering off the electron produces scattered light which travels along the z direction and has polarizations aligned with the x and y axes. The component of the scattered light which is polarized along the x direction (blue) originated from the (blue) incident photon which was travelling along the y direction. Similarly the (red) polarization component of the scattered light originated from the (red) photon incident along the x direction. If the incident radiation field has an overall quadrupole moment (i.e., if the magnitude of the red and blue intensities are not equal) then the scattered radiation will be polarized. For example, if the y–incident photon has a larger amplitude than the x–incident photon, we represent this graphically with longer blue lines than red lines. Then the scattered light also has longer blue lines than red and would be polarized along the x direction.

top of the page, and by imagining a photon propagating out of the page. If the photon has polarization along the N–S (E–W) direction we say that $Q > 0$ ($Q < 0$). On the other hand, if the photon is polarized along the NE–SW (NW–SE) direction, we say $U > 0$ ($U < 0$). The polarization can then be described in terms of a magnitude (P) and direction (α), which are given by

$$P = \sqrt{Q^2 + U^2} \qquad \alpha = \frac{1}{2} \arctan\left(\frac{U}{Q}\right). \tag{1.16}$$

One can also describe circular polarization in terms of the Stokes parameters, but we shall assume that circular polarization from cosmological sources is negligible.

The remainder of this thesis will focus on calculating the contribution to the CMB polarization power spectrum from cosmic string wakes. Chapter 2 will provide an introduction to spin–s fields and their importance for CMB polarization. We then introduce the flat sky approximation and simplify the spin–s equations greatly. In chapter 3, we begin calculating the contribution to the polarization power spectrum from cosmic string wakes, and we show that the total contribution can be given by a sum of contributions from individual wakes. We will derive an expression for the power spectrum contribution a single cosmic string wake. We then calculate the statistics from a network of cosmic string wakes in chapter 4. We outline the cosmic string scaling solution and use it to derive the statistics of the network for the purpose of calculating the full power spectrum contribution. We present the results of the calculation in chapter 5 and draw conclusions in chapter 6.

2

SPIN–s FIELDS

In this chapter we will discover that polarization fields transform non-trivially under a change of coordinates, and we will inroduce the technology of spin–s fields to correctly handle this behaviour. We will then make use of the flat sky approximation to simplify the resulting expressions.

In the context of the CMB, polarization is generated by Thomson scattering of photons originating from regions in the CMB with an overall temperature quadrupole. In order to succinctly describe the observed polarization map, we have at our disposal a number of representations from which to choose. In particular, we can choose between a complex scalar, a vector, or a tensor representation of the polarization[1]. Regardless of the representation, the interesting CMB polarization physics is captured entirely in only two of the Stokes parameters: Q and U[2].

1 It is interesting to contrast the approaches used in [28, 29, 30, 31]. However, it is important to keep track of the notation and conventions used by the different authors, as new students can easily become confused!

2 The V Stokes parameter corresponds to the intensity of circularly polarized light, which cannot be generated through Thompson scattering. Therefore, it is not particularly interesting for CMB polarization physics.

The Stokes parameters are not invariant under a change of coordinates and a rotation by an angle α transforms them via

$$\begin{aligned} Q' &= Q\cos(2\alpha) + U\sin(2\alpha) \\ U' &= U\cos(2\alpha) - Q\sin(2\alpha). \end{aligned} \tag{2.1}$$

As such, the polarization field is referred to as a spin–2 quantity, and we must maintain the correct transformation laws in whichever representation we choose. Since we are interested in a spin–2 field, it will prove useful to review some basic properties and simplifications for generic spin–s fields.

2.1 DEFINITIONS AND PRELIMINARIES

The concepts, conventions, and notations in this section are based on the excellent reference by Zaldarriaga and Seljak [28]. The curious reader is referred to Goldberg et al. [32] for more detail. A great deal of machinery exists for spin weighted fields in all three of the scalar, vector, and tensor representations. Since we are using the complex scalar representation, we will restrict our attention to spin–s functions and briefly review the spin raising and lowering differential operators, as well as small scale approximations.

Consider a unit sphere centered on the origin. Any point on the sphere can be parametrized using spherical coordinates in terms of (ϕ, θ). For a given point on the sphere, construct a tangent plane at that point and define two orthonormal unit vectors on the plane, $(\boldsymbol{e_1}, \boldsymbol{e_2})$. Define as well a third orthonormal vector to be the unit normal vector to the tangent plane, denoted by $\boldsymbol{n}$. Notice that $\boldsymbol{e_1}$ and $\boldsymbol{e_2}$ are only defined up to a rotation about $\boldsymbol{n}$.

Definition: A *spin–s* function ${}_sf(\phi,\theta)$ is one that, under a rotation of $(\boldsymbol{e_1},\boldsymbol{e_2})$ by an angle ψ about $\boldsymbol{n}$, transforms via

$$ {}_sf \to e^{-is\psi}{}_sf. \tag{2.2}$$

Borrowing an example from [28], the quantities $\boldsymbol{a}\cdot\boldsymbol{e_1}+i\boldsymbol{a}\cdot\boldsymbol{e_2}$, $\boldsymbol{a}\cdot\boldsymbol{n}$, and $\boldsymbol{a}\cdot\boldsymbol{e_1}-i\boldsymbol{a}\cdot\boldsymbol{e_2}$ for any $\boldsymbol{a}$ on the sphere have spin 1, 0, and -1 respectively. We pause briefly to recall that the stokes parameters Q and U rotate into one another twice when rotating a polarization map by an angle of 2π. Using the definition above, we conclude that the quantities $Q\pm iU$ are thus spin–±2.

2.2 SPIN RAISING AND LOWERING OPERATORS

Just as we have raising and lowering operators in the quantized treatment of angular momentum, we have spin raising and lowering operators in this complex scalar representation. Given a spin–s function, one can construct a spin–$(s+1)$ or spin–$(s-1)$ function via the action of differential operators. We define the *spin raising* and *spin lowering* operators, $\eth$ and $\bar{\eth}$, such that

$$(\eth_s f)' = e^{-i(s+1)\psi}(\eth_s f) \tag{2.3}$$

$$(\bar{\eth}_s f)' = e^{-i(s-1)\psi}(\bar{\eth}_s f) \tag{2.4}$$

under the same rotation of $(\boldsymbol{e_1},\boldsymbol{e_2})$ by an angle ψ, where prime represents the rotated function. The intuition behind $\eth$ and $\bar{\eth}$ is really as operators which raise or lower the spin of the function they take as argument. While this intuition

is crucial for solving problems, it is not so useful for performing computations, and we often rely on the explicit form:

$$\eth_s f(\phi,\theta) = -\sin^s(\theta)\left[\frac{\partial}{\partial\theta} + i\csc(\theta)\frac{\partial}{\partial\phi}\right]\sin^{-s}(\theta)\,{}_s f(\phi,\theta) \tag{2.5}$$

$$\bar{\eth}_s f(\phi,\theta) = -\sin^{-s}(\theta)\left[\frac{\partial}{\partial\theta} - i\csc(\theta)\frac{\partial}{\partial\phi}\right]\sin^{s}(\theta)\,{}_s f(\phi,\theta). \tag{2.6}$$

As is common with spin–0 fields, we can decompose our functions into a series solution (e.g., Taylor series, Fourier series, Laurent series, etc.). One convenient basis with which to decompose functions on a sphere is the spherical harmonics. A general function can be decomposed using the orthonormality of the spherical harmonics, Y_{lm} as

$$g(\phi,\theta) = \sum_{l,m} a_{lm} Y_{lm}(\phi,\theta), \tag{2.7}$$

where $g(\phi,\theta)$ is an arbitrary function over a region Ω of the sphere, and $a_{lm} = \int_\Omega g(\phi,\theta) Y^*_{lm}(\phi,\theta) d\Omega$. For spin–$s$ fields, generalizations of the spherical harmonics exist and provide natural bases with which to decompose higher spin weighted functions. Thus, the spin–s spherical harmonics, ${}_sY_{lm}$ form a complete basis for spin–s functions on the sphere.

As one would expect, we can construct spin–s spherical harmonics via the application of the spin raising and lowering operators to the regular scalar spherical harmonics. In particular,

$$\begin{aligned} {}_sY_{lm} &= \left[\tfrac{(l-s)!}{(l+s)!)}\right]^{\frac{1}{2}} \eth^s Y_{lm}\,, && (0 \le s \le l) \\ {}_sY_{lm} &= \left[\tfrac{(l+s)!}{(l-s)!)}\right]^{\frac{1}{2}} (-1)^s \bar{\eth}^{-s} Y_{lm}\,, && (-l \le s \le 0). \end{aligned} \tag{2.8}$$

2.3 THE SMALL ANGLE OR "FLAT SKY" APPROXIMATION

Having gone to great lengths to define the spin–s spherical harmonics, we will, with great pleasure, dispense with them as soon as possible. The reason for this is two–fold: observational cosmologists will agree that taking derivatives of data is ill–advised, while theorists appreciate the simplicity of scalar (spin–0) fields. Furthermore, when integrating over a small region of the sphere, orthogonality of spherical harmonics may not hold and the spin–0 spherical harmonics are much easier to work with. Fortunately, certain approximations allow us to convert a spherical harmonic expansion to an expansion in Fourier modes – a far tamer beast. The most appropriate simplification we can make stems from a physically relevant approximation. We assume that we are only interested in a very small region on the unit sphere (or sky), which allows us to use the small angle approximation. In terms of the celestial sphere, this is known as the "flat sky approximation", so–called because we neglect the curvature of the sphere in a small region and restrict our attention to the tangent plane.

Since we are interested in polarization – a spin–2 quantity – we shall focus on the spin–2 spherical harmonics. Applying the flat sky approximation gives

$$\begin{aligned} {}_2Y_{lm} &\simeq (2\pi)^{-2}\frac{1}{l^2}\eth^2 e^{i\boldsymbol{l}\cdot\boldsymbol{\theta}} \\ {}_{-2}Y_{lm} &\simeq (2\pi)^{-2}\frac{1}{l^2}\bar{\eth}^2 e^{i\boldsymbol{l}\cdot\boldsymbol{\theta}}, \end{aligned} \tag{2.9}$$

where $\boldsymbol{l} = (l_x, l_y)^\top$, and $\boldsymbol{\theta} = (\phi, \theta)^\top$. We further our approximation using the relations

$$\begin{aligned} \frac{1}{l^2}\eth^2 e^{i\boldsymbol{l}\cdot\boldsymbol{\theta}} &\simeq -e^{-2i(\phi-\phi_l)}e^{i\boldsymbol{l}\cdot\theta} \\ \frac{1}{l^2}\bar{\eth}^2 e^{i\boldsymbol{l}\cdot\boldsymbol{\theta}} &\simeq -e^{2i(\phi-\phi_l)}e^{i\boldsymbol{l}\cdot\theta}, \end{aligned} \tag{2.10}$$

where now $(l_x + il_y) = le^{i\phi_l}$.

Since the Stokes parameters Q and U rotate into one another under a rotation of coordinates (*c.f.* eq. (2.1)), we must take into account a desirable change of coordinates so that the flat sky approximation is applied to the "north pole" of the sphere and we work on the tangent plane perpendicular to the $\hat{\boldsymbol{z}}$ direction. In particular, our new Stokes parameters satisfy

$$(Q \pm iU)' = e^{\mp 2i\phi}(Q \pm iU). \tag{2.11}$$

Having properly accounted for the spin–weighting of polarization, we are well poised to set in on a computation of the polarization power spectrum.

3

THE POWER SPECTRUM

In this section, we describe the decomposition of polarization from a *single* wake into spin–2 spherical harmonics and apply the flat sky approximation.

3.1 E AND B MODES

In spherical coordinates (i.e., a metric $g_{ab} = \mathrm{diag}(1, \sin^2\theta)$), the (spin–2) polarization *tensor* can be written as

$$\mathcal{P}_{ab} = \frac{1}{2}\begin{pmatrix} Q(\hat{n}) & -U(\hat{n})\sin\theta \\ -U(\hat{n})\sin\theta & -Q(\hat{n})\sin^2\theta \end{pmatrix}, \tag{3.1}$$

while the polarization *vector* can be written as

$$\boldsymbol{P} = \begin{pmatrix} Q(\hat{n}) \\ U(\hat{n}) \end{pmatrix}, \tag{3.2}$$

and the (spin–2) complex scalar quantities of interest are $Q + iU$ and $Q - iU$. We will focus mainly on the scalar representation, making reference to the vector representation whenever helpful.

Referring to eq. (2.1), we see that for each cosmic string wake there exist coordinates in which $U = 0$. In other words, there exists a choice of α relating our chosen global coordinates to the convenient choice coordinates (in which $U = 0$) for each cosmic string wake. In particular,

$$\begin{aligned} Q' &= Q\cos(2\alpha) \\ U' &= -Q\sin(2\alpha) \end{aligned} \tag{3.3}$$

and we subsequently drop the primes.

We now decompose the spin–2 quantities $Q \pm iU$ using the spin–2 spherical harmonics. In particular, we have

$$\begin{aligned} (Q+iU)(\hat{\boldsymbol{n}}) &= \sum_{l=2}^{\infty}\sum_{m=-l}^{l} {}_2a_{lm}\,{}_2Y_{lm}(\hat{\boldsymbol{n}}) \\ (Q-iU)(\hat{\boldsymbol{n}}) &= \sum_{l=2}^{\infty}\sum_{m=-l}^{l} {}_{-2}a_{lm}\,{}_{-2}Y_{lm}(\hat{\boldsymbol{n}}). \end{aligned} \tag{3.4}$$

Note that we include contributions from $l \geq 2$ since any $l = 1$ dipole terms would be indistinguishable from the observed kinematic dipole. The coefficients, ${}_{\pm 2}a_{lm}$, are obtained by integrating against the spin–2 spherical harmonics as usual. It is common to define two new coefficients,

$$\begin{aligned} a_{E,lm} &= -\frac{1}{2}({}_2a_{lm} + {}_{-2}a_{lm}) \\ a_{B,lm} &= \frac{i}{2}({}_2a_{lm} - {}_{-2}a_{lm}), \end{aligned} \tag{3.5}$$

where the E and B represent “electric–type” and ”magnetic–type” components of the polarization. These coefficients are used to define rotationally invariant (spin–0) fields which completely characterize the polarization field. Thus, the E

and B fields have expansions in terms of the spin–0 spherical harmonics given by

$$E(\hat{\boldsymbol{n}}) = \sum_{l=2}^{\infty} \sum_{m=-l}^{l} a_{E,lm} Y_{lm}(\hat{\boldsymbol{n}}) \tag{3.6}$$

$$B(\hat{\boldsymbol{n}}) = \sum_{l=2}^{\infty} \sum_{m=-l}^{l} a_{B,lm} Y_{lm}(\hat{\boldsymbol{n}}). \tag{3.7}$$

Note that E and B are related to Q and U, but differ by derivatives. Nonetheless, E and B completely characterize the polarization field by breaking it into curl– and divergence–free components.

Our primary goal is to calculate the power spectrum in the CMB polarization due to cosmic string wakes. Since our principal observational target is the South Pole Telescope, we restrict our view to a small patch on the sky (e.g., $10^\circ \times 10^\circ$) corresponding to a single observational run. We therefore make the flat sky approximation and greatly simplify our calculations.

Combining eqs. (2.9) and (2.10) with eq. (3.4) and making the replacement $\sum_{l=2}^{\infty} \sum_{m=-l}^{l} \to \int d^2\boldsymbol{l}$ we have

$$\begin{aligned} (Q + iU) &\simeq -\frac{1}{(2\pi)^2} \int {}_2 a_{lm} e^{-2i(\phi - \phi_l)} e^{i\boldsymbol{l}\cdot\boldsymbol{\theta}} d^2\boldsymbol{l} \\ (Q - iU) &\simeq -\frac{1}{(2\pi)^2} \int {}_{-2} a_{lm} e^{2i(\phi - \phi_l)} e^{i\boldsymbol{l}\cdot\boldsymbol{\theta}} d^2\boldsymbol{l}, \end{aligned} \tag{3.8}$$

where again $\boldsymbol{l} = (l_x, l_y)^\top$ and $(l_x + i l_y) = l e^{i\phi_l}$

Using the definition of E and B, and taking eq. (2.11) into account, we finally arrive at

$$\begin{aligned} Q(\boldsymbol{\theta}) &\simeq \frac{1}{(2\pi)^2} \int [E(\boldsymbol{l}) \cos(2\phi_l) - B(\boldsymbol{l}) \sin(2\phi_l)] e^{i\boldsymbol{l}\cdot\boldsymbol{\theta}} d^2\boldsymbol{l} \\ U(\boldsymbol{\theta}) &\simeq \frac{1}{(2\pi)^2} \int [E(\boldsymbol{l}) \sin(2\phi_l) + B(\boldsymbol{l}) \cos(2\phi_l)] e^{i\boldsymbol{l}\cdot\boldsymbol{\theta}} d^2\boldsymbol{l}. \end{aligned} \tag{3.9}$$

Equation (3.9) illustrates the power of the flat sky approximation; not only have we shed the excess weight of spin–weighted functions and spherical harmonics, but we have also converted computationally difficult discrete sums to easy Fourier integrals.

Since we are interested in the E– and B–mode power spectra, we Fourier transform eq. (3.9) to get $\tilde{Q}$ and $\tilde{U}$ and undo the rotation to give

$$\begin{aligned} E(\boldsymbol{l}) &= \tilde{Q}(\boldsymbol{l})\cos(2\phi_l) + \tilde{U}(\boldsymbol{l})\sin(2\phi_l) \\ B(\boldsymbol{l}) &= -\tilde{Q}(\boldsymbol{l})\sin(2\phi_l) + \tilde{U}(\boldsymbol{l})\cos(2\phi_l). \end{aligned} \tag{3.10}$$

3.2 POLARIZATION FROM COSMIC STRINGS

By linearity, we have that the overall polarization field decomposes into a contribution from Gaussian fluctuations, and the sum of all contributions from individual string wakes. That is,

$$\boldsymbol{P} = \boldsymbol{P}^{\text{Gaussian}} + \sum_i \boldsymbol{P}^{\text{cs},i}, \tag{3.11}$$

where the sum is taken over all cosmic string wakes, labeled by i.

The magnitude of polarization, $\mathcal{P}^i$, was found by Danos et al. [21], but can be understood heuristically as follows. The strength of polarization coming from a cosmic string wake will depend on the number of free electrons in the wake that give rise to Thomson scattering. As such, we expect the magnitude of polarization to depend on the Thomson cross–section, σ_T, the number density of free electrons, the size of the wake, and the CMB temperature quadrupole, Q_{quad}.

The number density of free electrons in the wake at the time it was formed is given by

$$n_e(t_i) = f(t_i)\rho_B(t_i)m_p^{-1}, \tag{3.12}$$

where n_e is the number density of free electrons, f is the ionization fraction, ρ_B is the energy density in baryons, and m_p is the proton mass. Since the number density of free electrons redshifts as the universe expands, at the time the wake crosses our past light cone, the number density will be

$$n_e(t, t_i) = f(t)\rho_B(t_i)m_p^{-1}\left(\frac{z(t)+1}{z(t_i)+1}\right)^3. \tag{3.13}$$

We can express ρ_B in terms of the critical density $\rho_c(t_0)$ at the current time (t_0), the baryon fraction Ω_B, and appropriate redshift factors. The thickness of the wake is more complicated to compute, but Danos et al. [21] found that it is proportional to the speed of the cosmic string, v_s, the associated relativistic factor γ_s, the dimensionless quantity $G\mu$, and additional redshift factors.

Combining everything, the resulting magnitude of polarization is then found to be

$$\mathcal{P}^i = \frac{24\pi}{25}\left(\frac{3}{4\pi}\right)^{1/2}\sigma_T f G\mu v_s\gamma_s\Omega_B\rho_c(t_0)m_p^{-1}t_0(z(t)+1)^2(z(ti)+1)^{1/2}Q_{\text{quad}}, \tag{3.14}$$

where we have linearized in $G\mu$ and used the fact that the wake is thin with respect to the proper distance to the wake. Here, Q_{quad} is the CMB quadrupole today, and the redshift dependence of the quadrupole is already built into the expression.

In a frame with $U = 0$, we must have that $|\boldsymbol{P}| = Q$, and thus

$$\begin{aligned} Q^i &= \mathcal{P}^i \cos(2\alpha) \\ U^i &= -\mathcal{P}^i \sin(2\alpha). \end{aligned} \tag{3.15}$$

From eq. (2.1) we know that we can orient the wake such that Q and U are given by eq. (3.15). Thus, eq. (3.10) gives

$$\begin{aligned} E(\boldsymbol{l}) &= \tilde{\mathcal{P}}(\boldsymbol{l}) \left(\cos(2\phi_l)\cos(2\alpha) - \sin(2\phi_l)\sin(2\alpha)\right) \\ B(\boldsymbol{l}) &= -\tilde{\mathcal{P}}(\boldsymbol{l}) \left(\cos(2\phi_l)\sin(2\alpha) + \sin(2\phi_l)\cos(2\alpha)\right). \end{aligned} \tag{3.16}$$

Since we will eventually have to contend with a network of cosmic string wakes, we will inevitably have to deal with wakes oriented at different angles, α^i, with respect to the coordinate system chosen above. However, the power spectrum contains an ensemble average over all realizations of the wakes. As such, we will eventually integrate over the angles α and ϕ_l.

The reionization history of the universe is a tricky thing to nail down. Although a rough estimate of $f(t)$ would suffice for our purposes, we approximate the ionization history with the function shown in fig. 7. This function is an approximation to the ionization history given by Kaplinghat et al. [33].

The position space signature of polarization due to cosmic string wakes was determined by Danos et al. [21]. The effect of the cosmic string wake on the background matter is to cause an overdensity which accretes gravitationally, as was described in section 1.2. As such, we expect a rectangular patch with a linear fade in the polarization magnitude along the direction of travel of the string. We describe the angular size of the cosmic string wake in terms of two angles, d and w, corresponding to the angular length and width of the string. We let d describe the length of the wake so that the linear fade lies along this direction, while w describes the other wake dimension along which the

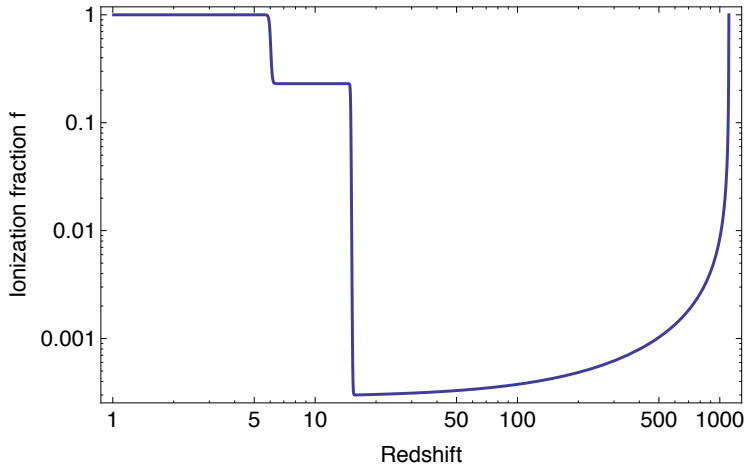

Figure 7: Reionization history of the universe up to the epoch of last scattering as a function of redshift. This function is an approximate version of the ionization history obtained in [33].

polarization is constant. In terms of these dimensions, the functional form of the polarization magnitude is given in the small–angle approximation by

$$\mathcal{P}(\boldsymbol{x}) = \mathcal{P}\Theta(|x| < \frac{d}{2})\Theta(|y| < \frac{w}{2})\left(\frac{2}{d}x + 1\right), \tag{3.17}$$

where Θ is the heaviside step function. An example of the polarization signal from a wake is shown in fig. 8 for particular values of the wake geometry. In general, our wakes will have a fixed aspect ratio (set by the scaling solution and numerical simulations), and will be rectangular. In Fourier space, the polarization magnitude is given by

$$\begin{aligned}\tilde{\mathcal{P}}(\boldsymbol{l}) &= \iint \mathcal{P}\Theta(|x| < \frac{d}{2})\Theta(|y| < \frac{w}{2})\left(\frac{2}{d}x + 1\right) e^{-il_x x} e^{-il_y y} dxdy \\ &= \mathcal{P}\int_{-\frac{d}{2}}^{\frac{d}{2}}\int_{-\frac{w}{2}}^{\frac{w}{2}}\left(\frac{2}{d}x + 1\right) e^{-i(l_x x + l_y y)} dxdy \\ &= \frac{4\sin\left(\frac{l_y w}{2}\right)\left\{il_x d\cos\left(\frac{l_x d}{2}\right) + (-2i + l_x d)\sin\left(\frac{l_x d}{2}\right)\right\}}{l_x^2 l_y d}.\end{aligned} \tag{3.18}$$

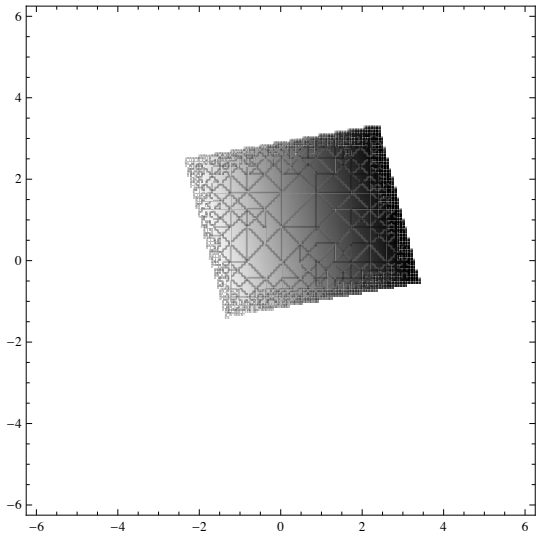

Figure 8: An example of a cosmic string wake for chosen values of the offset angle, position, orientation, etc.

3.3 THE POWER SPECTRUM

The definition of the full sky angular power spectrum is

$$C_l = \frac{1}{2l+1} \sum_{m=-l}^{l} \langle a_{lm} a_{lm}^* \rangle, \tag{3.19}$$

where a_{lm} is the coefficient in front of the spherical harmonic Y_{lm} in the decomposition for any field of interest (E, B, T), while $\langle \cdots \rangle$ means ensemble average of the input. For us, the averaging is done over the polarization angle α, positions of the wakes on the sky, and any other parameters. Rather than computing the full angular power spectrum, we will instead compute the flat sky analog, which agrees to a good approximation over the small flat sky patch [34, Appendix C]. In the flat sky approximation, the power spectrum is given by

$$C_l^{XX} = \langle X(l) X(l)^* \rangle, \tag{3.20}$$

where $X \in \{E, B, Q, U, \dots\}$.

We are interested in an integrated effect of many wakes within a single observational patch. Thus, by linearity,

$$\tilde{\mathcal{P}}(\boldsymbol{l}) = \sum_{i=1}^{N} \tilde{\mathcal{P}}(\boldsymbol{l})^i, \tag{3.21}$$

where N is the total number of wakes. We use the ensemble averaging to enforce statistical independence of the cosmic string wakes. In other words, the total power spectrum is a sum over the individual power spectra for single wakes. While it arises naturally, this independence can be achieved artificially by inserting into the polarization magnitude a variable ξ_i with the property that $\langle \xi_i \xi_j \rangle = \delta_{ij}$. Then

$$\left\langle \tilde{\mathcal{P}}^i \xi^i \, \tilde{\mathcal{P}}^{j,*} \xi^j \right\rangle = \left\langle \tilde{\mathcal{P}}^i \tilde{\mathcal{P}}^{j*} \right\rangle \langle \xi^i \xi^j \rangle = \left\langle \left| \tilde{\mathcal{P}}^i \right|^2 \right\rangle. \tag{3.22}$$

More concretely, the same statistical independence arises when performing the ensemble average over α. For example,

$$C_l^{EE} = \left\langle \left(\sum_{i=1}^{N} E^i \right) \left(\sum_{j=1}^{N} E^j \right)^* \right\rangle. \tag{3.23}$$

Inserting the form of E from eq. (3.16) and expanding the sums leaves us with terms of the form

$$\left\{ \begin{array}{c} \cos(2\alpha^i)\cos(2\alpha^j)\cos(2\phi_l^i)\cos(2\phi_l^j) \\ \sin(2\alpha^i)\sin(2\alpha^j)\sin(2\phi_l^i)\sin(2\phi_l^j) \\ \sin(2\alpha^i)\cos(2\alpha^j)\cos(2\phi_l^i)\sin(2\phi_l^j) \\ \vdots \end{array} \right\}. \tag{3.24}$$

When taking the ensemble average over α, we note that

$$\begin{aligned}
\left(\frac{1}{2\pi}\right)^2 \int_0^{2\pi}\int_0^{2\pi} \cos(2\alpha^i)\cos(2\alpha^j)d\alpha^i d\alpha^j &= \frac{1}{2}\delta(\alpha^i-\alpha^j)\\
\left(\frac{1}{2\pi}\right)^2 \int_0^{2\pi}\int_0^{2\pi} \sin(2\alpha^i)\sin(2\alpha^j)d\alpha^i d\alpha^j &= \frac{1}{2}\delta(\alpha^i-\alpha^j)\\
\left(\frac{1}{2\pi}\right)^2 \int_0^{2\pi}\int_0^{2\pi} \sin(2\alpha^i)\cos(2\alpha^j)d\alpha^i d\alpha^j &= 0
\end{aligned} \tag{3.25}$$

so that cross–terms corresponding to two different wakes with $\alpha^i \neq \alpha^j$ and cross–terms of the form $\cos(2\alpha^i)\sin(2\alpha^j)$ vanish. Once the dust settles, the averaging leaves us with

$$\begin{aligned}
C_l^{EE} &= \left\langle \sum_i \frac{1}{2}\left|\tilde{\mathcal{P}}^i\right|^2 \left(\cos^2(2\phi_l^i)+\sin^2(2\phi_l^i)\right)\right\rangle\\
&= \left\langle \sum_i \frac{1}{2}\left|\tilde{\mathcal{P}}^i\right|^2 \right\rangle\\
C_l^{EE} &= \sum_i \left(\frac{1}{4\pi}\right)\int_0^{2\pi}\left|\tilde{\mathcal{P}}^i\right|^2 d\phi_l^i,
\end{aligned} \tag{3.26}$$

where ϕ_l^i is the angle containing the spin–2 information about the orientation of wake i with respect to our chosen coordinates, and $\tilde{\mathcal{P}}$ is given by eq. (3.18). Note that rotating the wakes to coincide with one another affects the phase of the Fourier transforms of each wake and hence the associated m–modes. However, summing over m removes this orientation dependence. Since the positions of the wakes are uncorrelated, the full power spectrum really is the sum of the contributions from each wake. Furthermore, the position dependence of $Q_{\rm quad}$ from wake to wake washes out when taking the average, allowing us to use the average quadrupole value today for all wakes (since the redshift dependence is already built into $\mathcal{P}$).

Similarly, for the B field we have

$$C_l^{BB} = \sum_i \left(\frac{1}{4\pi}\right) \int_0^{2\pi} \left|\tilde{\mathcal{P}}^i\right|^2 \, d\phi_l^i. \tag{3.27}$$

It is also straightforward to check that $C_l^{EB} = 0$ by exact cancellation after averaging over α. Finally, $C_l^{ET} = 0 = C_l^{BT}$ because the temperature map is a spin–0 quantity and is thus independent of α. As such, averaging the ET and BT terms over α gives zero. Therefore, we arrive at our first non–trivial result: **the E–mode and B–mode power spectra from cosmic string wakes are equal, while all cross–correlations vanish:**

$$C_l^{EE} = C_l^{BB} \tag{3.28}$$

$$C_l^{EB} = C_l^{ET} = C_l^{BT} = 0. \tag{3.29}$$

Intuitively, the cross-correlation terms are non–zero in *position space*. However, these correlations arise with different signs for different wakes. As such, when computing a correlation function that is linear in E or B (ET or BT), these correlations average to zero and the correlation function vanishes.

We can estimate the amplitude of the power spectrum from a rough approximation of eq. (3.14). Using numerical values for ρ_c, σ_T, m_p, and t_0, and normalizing the redshift terms to values of 10^3, we have

$$\frac{\mathcal{P}}{Q_{quad}} \simeq f G\mu v_s \gamma_s \Omega_B \left(\frac{z(t)+1}{10^3}\right)^2 \left(\frac{z(t_i)+1}{10^3}\right)^{1/2} 10^7. \tag{3.30}$$

To get an order of magnitude estimate, we set $v_s\gamma_s \sim 1$ and approximate $f(t) = f(t_{ls}) \sim 1$ while the redshift terms are both of order unity for early times. Thus, $\frac{P}{Q} \sim \Omega_B$ for $G\mu \sim 10^{-7}$.

4

A COSMIC STRING NETWORK

In chapter 3 we found that we can break the full power spectrum into a sum over power spectra from individual wakes. We would now like to use the statistics of the scaling solution for a network of cosmic strings to assign a weight to the power spectra of individual wakes as a function of t and t_i. In particular,

$$C_l = \sum_t \sum_{t_i} N_w(t, t_i) C_l(t, t_i), \tag{4.1}$$

where $N_w(t, t_i)$ is the number of wakes laid down at time t_i that intersect our past light cone at time t, and the sums are taken over discrete Hubble time steps. In order to calculate N_w, we must first review some basics of the scaling solution for cosmic strings.

4.1 THE SCALING SOLUTION

A detailed analysis of the evolution of a network of cosmic strings gives rise to a simple, yet powerful result: the network of cosmic strings approaches a scaling solution [35]. This means that all statistical properties of the network become time independent when all lengths are scaled by the Hubble length. In other words, if we know the distribution of cosmic strings at some time t_1, we

can find the distribution and properties of the network at another time t_2 by converting all distances with the appropriate factors of the Hubble length. As such, the number of cosmic strings per Hubble volume, n_w, remains constant in time when all lengths are appropriately scaled.

In a network of cosmic strings, one can define a correlation length ζ characterizing the rough length scale over which long strings are correlated. ζ also tends to correspond roughly to the radius of cosmic string loops at formation. In the scaling solution, one finds that $\zeta \sim t$, so that it remains constant when scaled by the Hubble length. Thus, the rough length of a long cosmic string in the scaling solution is about one Hubble volume.

Since all statistics of the cosmic string network are constant in time when lengths are scaled to the Hubble length, we can greatly simplify numerical simulations of the evolution of a cosmic string network by discretizing time into Hubble time steps. In other words, we can run simulations for one Hubble time, reset all parameters according to the scaling solution, then run the simulation for another Hubble time. This is tantamount to initializing a network of cosmic strings with lengths on the order of the Hubble length, running a simulation for one Hubble time step, then re–initializing the simulation with a new network of cosmic strings according to the scaling solution. Since all statistics are time independent, we can rest assured that any statistical properties we calculate will remain invariant when re–initializing.

As mentioned in earlier sections there are two types of strings in a cosmic string network: long strings and loops. Wakes generated by long strings have more distinct position space features than loops, and it is these signatures that we have chosen to study. However, it should be noted that loops will decay via gravitational radiation and other effects [5], which can give rise to polarization

from gravitational waves. Nonetheless, we will focus on the contribution from long strings alone.

4.2 STRING STATISTICS

Armed with the scaling solution, we convert the physical parameters in the problem to functions of t_i and t.

Angular size

The angular size of the wake is given by the ratio of the size of the string to its distance to us, making use of the small angle approximation. In comoving coordinates, we denote the length of the string by ℓ_c, and the distance to it by $\eta_0 - \eta(t_i)$ (in natural units), where η is conformal time and η_0 is now. Since we are only interested in times after equal matter–radiation, we approximate the universe as matter dominated. As such, the scale factor is always

$$a(t) = \left(\frac{t}{t_0}\right)^{2/3}. \tag{4.2}$$

Since ℓ_c is one Hubble length in comoving coordinates, we have

$$\begin{aligned} \ell_c &= \frac{1}{H(t_i)}\frac{1}{a(t_i)} \\ &= \frac{3t_i}{2}\left(\frac{t_0}{t_i}\right)^{2/3} \\ &= \frac{3}{2}t_0\left(\frac{t_i}{t_0}\right)^{1/3}, \end{aligned} \tag{4.3}$$

and the difference in conformal time can be calculated by integrating the definition $dt = a(t)d\eta$ to get

$$\begin{aligned}\eta_0 - \eta(t_i) &= \int_t^{t_0} \frac{dt'}{t'^{2/3}} t_0^{2/3} \\ &= 3t_0^{2/3}(t_0^{1/3} - t^{1/3}) \\ &= 3t_0\left(1 - \left(\frac{t}{t_0}\right)^{1/3}\right). \end{aligned} \tag{4.4}$$

Combining the two gives us an expression for the angular size

$$\omega(t_i, t) = \frac{\ell_c}{\eta_0 - \eta(t_i)} = \frac{(t_i/t_0)^{1/3}}{2(1 - (t/t_0)^{1/3})}. \tag{4.5}$$

In the scaling solution, the direction parallel to the string has an average

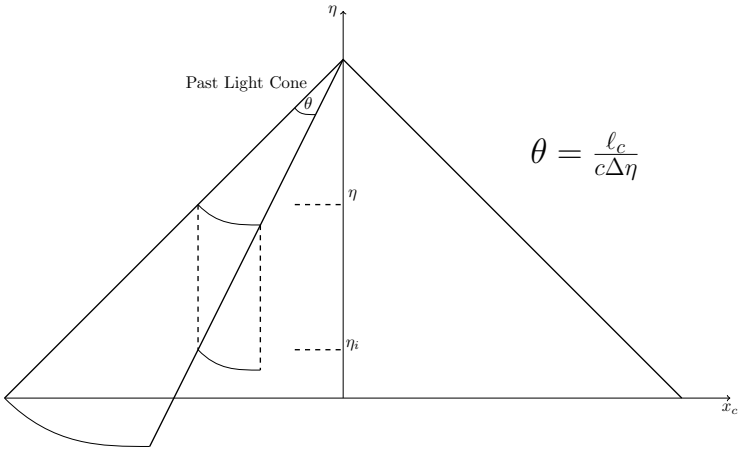

Figure 9: Conformal spacetime diagram showing the angular size of cosmic string wakes.

length on the order of one Hubble length, so we set that direction equal to $c_1\ell_c$. The direction perpendicular to the string is the direction in which the string moves. As such, wakes will have a comoving length given by $v_s\gamma_s\ell_c$. Therefore, we arrive at the following replacements:

$$d \to d(t_i, t) = v_s\gamma_s\omega(t_i, t) \qquad w \to w(t_i, t) = c_1\omega(t_i, t). \tag{4.6}$$

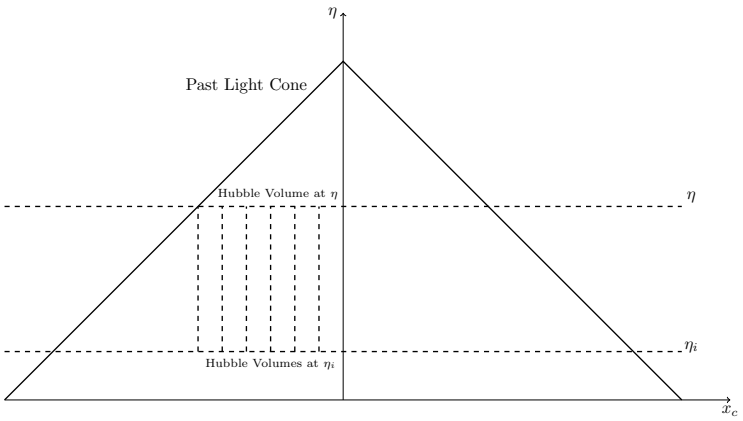

Figure 10: Conformal spacetime diagram showing the intersection of early wakes with the past light cone.

We now compute $N_w(t, t_i)$, the number of wakes laid down at t_i that intersect the past light cone at time t. From the scaling solution, we know that there are n_w wakes laid down per Hubble time per Hubble volume, where $0 < n_w < 10$ is a fixed constant that can be obtained from numerical simulations. Thus, the number of wakes that intersect our past light cone (PLC) at time t is n_w times the number of Hubble volumes at time t_i that fit inside the observed volume of our past light cone in one Hubble time around time t, summed over discrete Hubble times t_i. Mathematically,

$$N_w(t, t_i) = n_w \frac{\text{Vol(PLC)}_{\text{com}}(t)}{\text{Vol(Hubble)}_{\text{com}}(t_i)}. \tag{4.7}$$

Figure 10 shows the way we count the number of strings laid down at time t_i which intersect at t.

Hubble volume

The physical Hubble volume at time t_i is $\frac{4}{3}\pi R_H^3$ where R_H is the Hubble radius. Thus, the comoving Hubble volume is given by

$$\begin{aligned}\text{Vol(Hubble)}_{\text{com}} &= \frac{\frac{4}{3}\pi R_H^3}{a(t_i)^3} \\ &= \frac{4}{3}\pi\left(\frac{1}{H(t_i)}\right)^3 \frac{1}{a(t_i)^3} \\ &= \frac{4}{3}\pi \dot{a}(t_i)^{-3} \\ &= \frac{4}{3}\pi\left(\frac{3t_0}{2}\right)^3 \left(\frac{t_i}{t_0}\right) \\ &= \frac{9\pi}{2} t_0^2 t_i. \end{aligned} \tag{4.8}$$

Comoving volume of the past light cone

In order to compute the volume of the past light cone, we first note that null geodesics satisfy

$$ds^2 = 0 = dt^2 - a^2(t) d\boldsymbol{x}^2. \tag{4.9}$$

This leads to the canonical definition of *comoving distance*

$$\ell = \int_t^{t_0} \frac{dt'}{a(t')}. \tag{4.10}$$

Note that in comoving coordinates, ℓ is simply $\eta_0 - \eta(t)$.

Substituting the matter dominated scale factor and integrating leads to a comoving distance of $3t_0(1 - a(t)^{1/2})$. Then the physical volume of the observed

portion of the past light cone between time t and one Hubble time after t (i.e., time $t + H^{-1}(t)$) is given by

$$\mathrm{Vol(PLC)}_{\mathrm{com}} = \left(\int d\Omega\right) \frac{\ell^3(t) - \ell^3(t + 3t/2)}{3}. \tag{4.11}$$

The solid angle contained in an observation volume parametrized by angles θ_1 and θ_2 is easily seen to be

$$\begin{aligned}
\int d\Omega &= \int \sin\theta d\theta d\phi \\
&= \int_{\theta_1/2}^{\theta_1/2} d\phi \int_{\pi/2-\theta_2/2}^{\pi/2+\theta_2/2} \sin\theta d\theta \\
&= \theta_1(\cos(\pi/2 - \theta_2/2) - \cos(\pi/2 + \theta_2/2)) \\
&= \theta_1(2\sin(\theta_2/2)) \simeq \theta_1\theta_2,
\end{aligned} \tag{4.12}$$

where θ_1 and θ_2 are small (and are approximately 10° each for SPT). This leaves us with

$$\mathrm{Vol(PLC)}_{\mathrm{com}} = 9\theta_1\theta_2 t_0^3 \left((1 - a(t)^{1/2})^3 - (1 - a(t + 3t/2)^{1/2})^3\right). \tag{4.13}$$

As mentioned above, the sum over wakes is done in discrete Hubble time steps, in accordance with the scaling solution. The Hubble time is defined to be $H(t)^{-1}$. Therefore the first Hubble time step, τ_0, begins at $\tau_0 = H(t_{init})^{-1}$, while the second is at $\tau_1 = 2\tau_0$, and the third is at $\tau_1 = 2\tau_1$, etc. Thus, the $n-$th Hubble time step is at $\tau_n = 2^n\tau_0$, or

$$\tau_n = \frac{2^n}{H(t_{init})}. \tag{4.14}$$

Since we are summing from the epoch of equal matter and radiation up to the present day for t_i, and from the surface of last scattering up to the present day for t, we need a maximum of

$$\begin{aligned}\frac{1}{H(t_0)} &= \frac{2^{n_{max}}}{H(t_{rm})} \\ \Rightarrow n_{max} &= \left\lfloor -\frac{3}{2}\log_2 a(t_{rm}) \right\rfloor \\ &= \left\lfloor +\frac{3}{2}\log_2(z_{rm}+1) \right\rfloor \\ &\sim \left\lfloor \frac{3}{2}\log_2(3600) \right\rfloor \\ &= 17 \end{aligned} \tag{4.15}$$

time steps in the t_i sum, and at most

$$\begin{aligned}\frac{1}{H(t_0)} &= \frac{2^{n_{ls}}}{H(t_{ls})} \\ \Rightarrow n_{max} &= \left\lfloor -\frac{3}{2}\log_2 a(t_{ls}) \right\rfloor \\ &= \left\lfloor +\frac{3}{2}\log_2(z_{ls}+1) \right\rfloor \\ &\sim \left\lfloor \frac{3}{2}\log_2(1100) \right\rfloor \\ &= 15 \end{aligned} \tag{4.16}$$

time steps in the t sum, where $\lfloor \cdots \rfloor$ is the floor function. However, breaking the volume into discrete chunks includes the present day in the last time step, and we only need to sum up to $n_{max} - 1$. Since we cannot see beyond the surface of last scattering, nor can we see a wake before it was formed, we need to start the sum over intersection times at t_{ls} whenever $t_i < t_{ls}$ and at t_i when $t_i > t_{ls}$. Converting the sum over t to have a common denominator one easily finds

$$\frac{2^{n_1}}{H(t_{ls})} = \frac{2^{n_1+n_{max}-n_{ls}}}{H(t_{rm})}. \tag{4.17}$$

Defining $n_1' = n_1 + n_{max} - n_{ls}$, it is clear that we start the sum over n_1' at $\max(n_2, n_{max} - n_{ls})$ and end at n_{max}. We subsequently drop the prime. Combining the volumes computed above, we have

$$\begin{aligned} N_w(t, t_i) &= n_w \frac{\text{Vol(PLC)}_{\text{com}}}{\text{Vol(Hubble)}_{\text{com}}} \\ &= n_w \frac{9\theta_1\theta_2 t_0^3 \left((1 - a(t)^{1/2})^3 - (1 - a(t + 3t/2)^{1/2})^3 \right)}{\frac{9\pi}{2} t_0^2 t_i} \\ &= n_w \frac{2\theta_1\theta_2}{\pi} \left(\frac{t_0}{t_i} \right) \left((1 - a(t)^{1/2})^3 - (1 - a(t + 3t/2)^{1/2})^3 \right). \end{aligned} \quad (4.18)$$

We then convert to discrete Hubble time steps with the substitutions $t \to 2^{n_1} H(t_{init})^{-1}$ and $t_i \to 2^{n_2} H(t_{init})^{-1}$. N_w is shown in fig. 11 as a function of n_1 for various choices of n_2. It is clear that N_w achieves a maximum as $n_2 \to 0$.

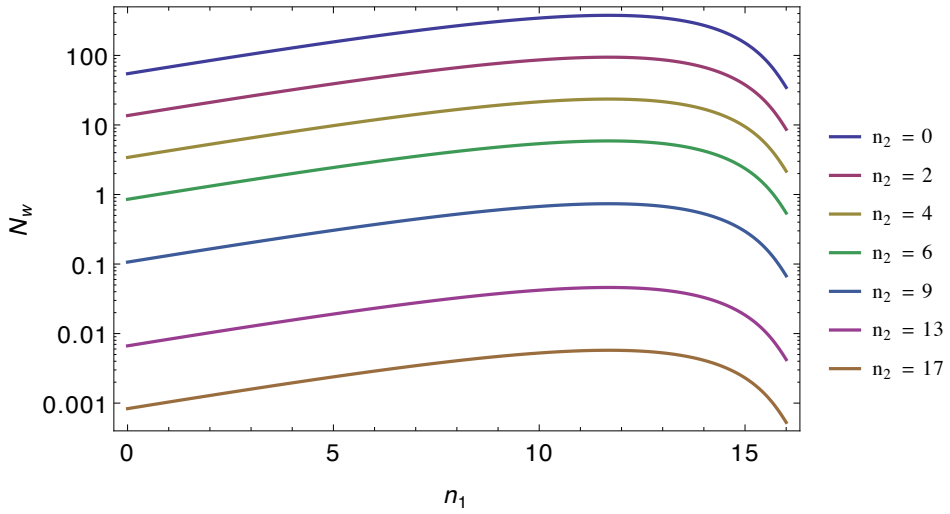

Figure 11: N_w as a function of n_1 for different values of n_2. Curves with larger amplitude correspond to smaller values of n_2. As such, n_2 simply rescales N_w with a maximum being obtained as $n_2 \to 0$. Thus, the maximum value of N_w occurs when $n_2 = 0$.

From the form of N_w, one might naively expect the dominant wakes to be formed at early times and intersect the past light cone at late times, since these wakes would have had more time to accrete gravitationally and would corre-

spond to a large angular size on the sky. However, there are other competing effects from the magitude of polarization and from the ionization fraction. One can see from the redshift dependence of eq. (3.14) that the largest magnitude of polarization comes from those wakes with the earliest formation and intersection times. Furthermore, from the size of N_w it is clear that terms of the form $(z+1)^2$ and $(z_i+1)^{1/2}$ will be the dominant contributions. As such, we expect the dominant contribution to come from those wakes $n_2 = 0$ (corresponding to wakes that were laid down at early times) and $n_1 \simeq 2$ (corresponding to wakes intersecting the past light cone at recombination). These wakes were formed at the earliest times and become visible as early as possible around the time of last scattering. Therefore, we expect the shape of the power spectrum to be influenced by the angular size of Hubble length features at these times.

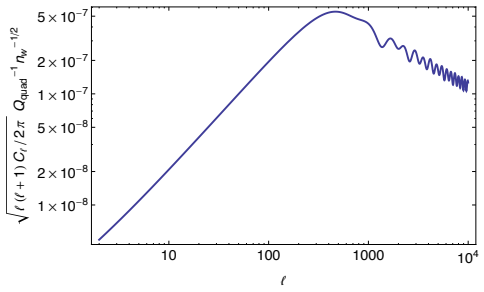

(a) $[l(l+1)C_l/2\pi]^{1/2}$ vs l for a dominant wake.

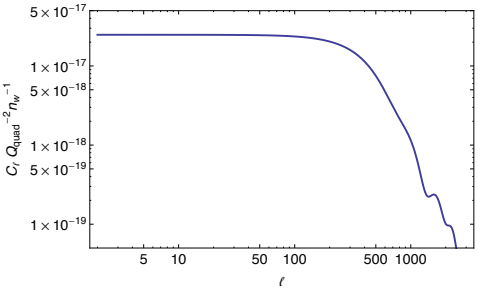

(b) C_l vs l for a dominant wake.

Figure 12: Example power spectra (log–log) showing both $\sqrt{l(l+1)C_l/2\pi}$ and C_l for choices of d and w corresponding to a single wake formed at equal matter radiation and intersecting the past light cone at recombination.

Putting everything together, we arrive at the final result

$$C_l = \sum_{n_2=0}^{n_{max}} \sum_{n_1>n_2}^{n_{max}} N_w(n1, n2) C_l \left(\frac{2^{n_1}}{H(t_{rm})}, \frac{2^{n_2}}{H(t_{rm})} \right), \tag{4.19}$$

with

$$C_l(t,t_i) = \frac{16}{4\pi d^2 l^6}\int \frac{\sin^2\left[\frac{1}{2}lw\sin\phi_l\right]}{\sin^2\phi_l\cos^4\phi_l}\{2-2\cos[ld\cos\phi_l] + ld\cos\phi_l(ld\cos\phi_l - 2\sin(ld\cos\phi_l))\}\,d\phi_l, \tag{4.20}$$

where all other functions have been defined above. Example power spectra for a single wake (i.e., neglecting the sum) are shown in figs. 12a and 12b where, incidentally, we've chosen a dominant wake.

5

RESULTS

In this chapter, we combine the results from all previous chapters to calculate the entire contribution to the CMB polarization power spectrum from cosmic string wakes. With a power spectrum in hand, we analytically verify the asymptotic behaviour (very small and very large ℓ). We further this analytic understanding by determining which wakes in the scaling solution provide the dominant contribution to the power spectrum.

Current observations of CMB polarization include signals from a number of sources. Since E–mode polarization can be produced by Gaussian fluctuations and B–mode polarization cannot, we will focus on B–mode polarization. The two dominant sources of B–mode polarization are gravitational lensing and gravitational waves. Although inflationary physics does not predict direct B–mode polarization from Gaussian fluctuations, it does predict a stochastic background of gravitational waves [36, 37]. This background can act to distort the CMB and can produce B–mode polarization [38] with a rough peak amplitude in the dimensionless power spectrum which can be estimated to be around 10^{-3} at $l \sim 100$. The second source of B–mode polarization is from gravitational lensing [39]. As with gravitational waves, the distortion of CMB photons by gravitational lensing can act to produce B–mode polarization with a rough peak amplitude in the dimensionless power spectrum of about 10^{-2}

at $l \sim 1000$. Having computed the power spectrum from polarization due to cosmic string wakes, we are in a position to compare with the predicted power spectra from gravitational waves and gravitational lensing.

5.1 COMBINED POWER SPECTRA

With all ingredients in hand we finally arrive at the CMB polarization power spectra for a network of cosmic string wakes. The results are shown in figs. 13 and 14. One important feature of fig. 13 (for both EE and BB) is that the

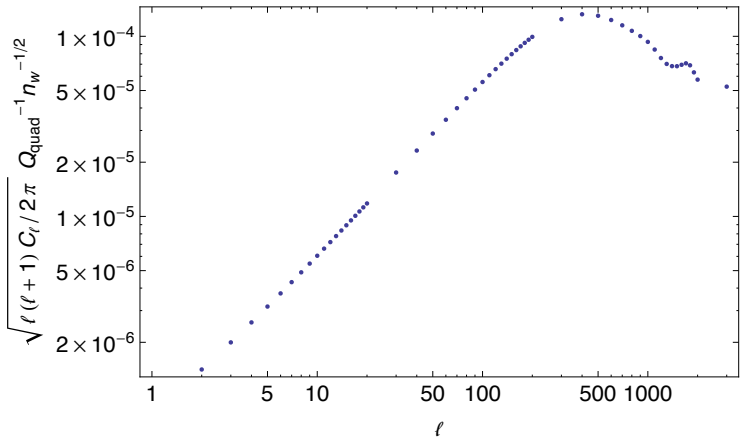

Figure 13: The CMB polarization power spectrum (EE or BB) for a network of cosmic string wakes. The EE and BB power spectra are equal in shape and magnitude, while the cross–correlation terms vanish.

power spectrum grows linearly in l for small l, with a turn around point at about $l \simeq 400$. This corresponds to a flat curve in fig. 14 for small l. Another feature is that the amplitude of the power is very low – too low to be detected and well within the signals from other sources. Furthermore, the shape of the power spectrum is very similar to that of gravitational lensing. As such, we conclude that the Fourier space signature of cosmic string wakes in CMB polarization is weak; we should focus our efforts on the distinct position space signature.

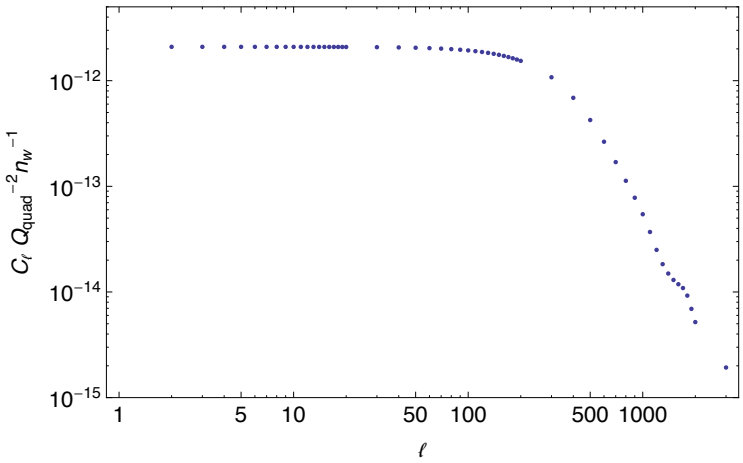

Figure 14: C_l vs l including the contribution from all wakes.

5.2 ASYMPTOTICS

Having calculated the polarization power spectrum, we aim to understand the physics governing the shape. For small l, we expand the expression for C_l in terms of $ld \ll 1$ ad $lw \ll 1$ giving

$$C_l \simeq \frac{\mathcal{P}}{2}(dw)^2, \qquad l < \frac{1}{d} \text{ and } l < \frac{1}{w} \tag{5.1}$$

for a single wake. Thus, the linear shape for small l seems natural. The power spectrum goes as the square of the area of the wake until we reach values of l corresponding to scales smaller than the size of the wake. When $l \sim \frac{1}{d}$, the Riemann–Lebesgue lemma becomes applicable and the averaging over ϕ_l causes the power spectrum to decrease. For very large l, we expect the rapid oscillations to average to zero giving $C_l \to 0$ as $l \to \infty$. Therefore, the power spectrum will be linear until we reach values of l corresponding to the angular size of the dominant wakes in the sum, at which point it will decay toward zero. Thus, it is important to find the dominant wakes.

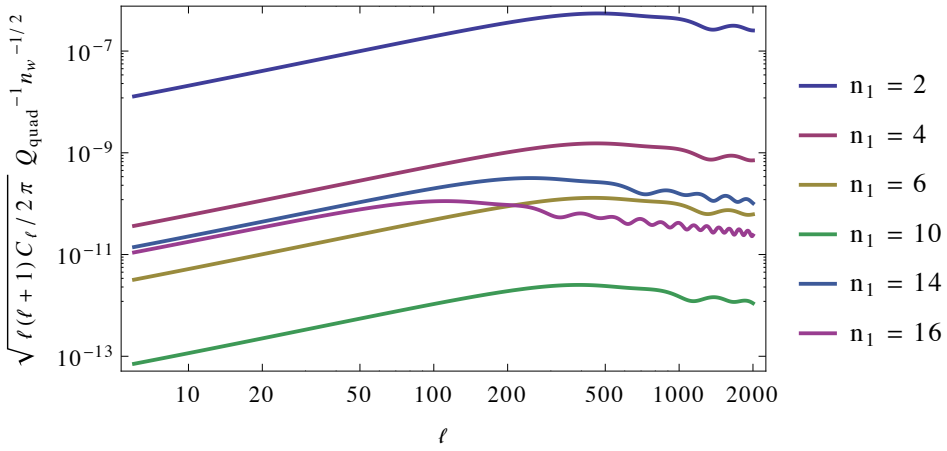

Figure 15: $[l(l+1)C_l/2\pi]^{1/2}$ vs l for wakes laid down at the epoch of equal matter and radiation, and intersecting the past light cone after n_1 Hubble time steps. Note that $n_1 = 2$ corresponds to recombination.

5.3 DOMINANT WAKES

We expect the dominant wakes to be those which maximize the quantity

$$N_w(t, t_i)\mathcal{P}(t, t_i)f(t). \tag{5.2}$$

As we have seen, these wakes correspond to those which were formed during the epoch of equal matter–radiation ($t_i = t_{rm}$), and those which intersect the past light cone earliest. Since we cannot see past the surface of last scattering, the dominant wakes will be those which intersect at recombination. This is evident in fig. 15 where we plot the power spectra of wakes formed at t_{rm} and intersecting our past light cone at various times. Thus, the combined power spectrum from the entire network of cosmic string wakes will be well approximated by the contribution from a single wake that formed very early and underwent Thomson scattering during recombination (see fig. 12). The angular size of such wakes corresponds to a turn around point in the power spectrum of $l \sim 400$, consistent with our findings.

6

CONCLUSIONS

We computed the angular power spectrum of CMB polarization due to a network of cosmic string wakes. Working in the flat–sky approximation, we found an expression for the power spectrum which shows that the EE and BB power spectra were equal in shape and magnitude. This result is consistent with other studies [21] in which it was found that cosmic strings produce B–mode polarization at leading order. Although this result is promising (because inflationary Gaussian fluctuations cannot directly produce B–mode polarization), the B–mode signal from gravitational lensing washes out any potential signal from cosmic string wakes [20]. Furthermore, the cross–correlation power spectra (e.g., ET, BT, and EB) vanish completely, and the shape of the BB power spectrum matches that of lensing, rendering the cosmic string signal nearly indistinguishable from that of gravitational lensing.

Weak signals aside, we found that the dominant contribution to the power spectrum comes from those wakes which were formed very early and insersect our past light cone very early as well. The earliest formation time in our model corresponds to $t_i = t_{eq}$ (formation at the time of equal matter and radiation), while the earliest possible intersection with our past light cone corresponds to wakes we observe on the last scattering surface ($t = t_{ls}$.) These wakes

dominate the power spectrum and set the amplitude and scale at which the power spectrum turns over (see fig. 13). As such

$$\begin{aligned} C_l^{Tot} &= \sum_{t,t_t} N_w(t,t_i) C_l(t,t_i) \\ &\sim C_l(t_{ls}, t_{eq}). \end{aligned} \tag{6.1}$$

We also found asymptotic limits of the power spectrum with the $l \to \infty$ limit sending $C_l \to 0$. The more interesting case is the small l limit in which

$$C_l \longrightarrow \frac{\mathcal{P}^2}{2}(dw)^2 \qquad l \lesssim \frac{1}{d}. \tag{6.2}$$

Combining this with the finding of the dominant wakes above, we finally conclude that the dimensionless power spectrum (C_l/Q_{quad}^2) remains flat with an amplitude of

$$\frac{1}{2}\frac{\mathcal{P}^2(t_{ls}, t_{eq})}{Q_{quad}^2}\left(d(t_{ls}, t_{eq}) w(t_{ls}, t_{eq})\right)^2 \simeq 2.5 \times 10^{-17} \tag{6.3}$$

until a maximum value of l corresponding to

$$l \sim \frac{2}{d} \simeq 350, \tag{6.4}$$

at which point the Riemann–Lebesgue lemma becomes applicable and we see that C_l begins to decay. In terms of the more physical quantity

$$\Delta B \simeq \sqrt{l(l+1)C_l^{BB}/2\pi Q_{quad}^2}, \tag{6.5}$$

we see from above that the power spectrum (i.e., $\sqrt{l(l+1)C_l/2\pi}$) grows linearly in l until a maximum value of about $l \sim 400$ and a peak amplitude of about 10^{-4}.

In conclusion, the Fourier space power in polarization from cosmic string wakes is too small to be detected above the background of gravitational lensing. However, the position space signature of cosmic string wakes is highly non–Gaussian and a more promising search for polarization from cosmic strings would make use of position space features. The rectangular signature found by Danos et al. [21] affords the use of edge detection algorithms (e.g., the Canny algorithm) which may lead to detection of cosmic strings in the future.

REFERENCES

[1] Georges Aad et al. Observation of a new particle in the search for the Standard Model Higgs boson with the ATLAS detector at the LHC. *Phys.Lett.*, B716:1–29, 2012.

[2] N. D. Mermin. The topological theory of defects in ordered media. *Rev. Mod. Phys.*, 51:591–648, Jul 1979.

[3] Ya.B. Zeldovich, I. Yu. Kobzarev, and L.B. Okun. Cosmological Consequences of the Spontaneous Breakdown of Discrete Symmetry. *Zh.Eksp.Teor.Fiz.*, 67:3–11, 1974.

[4] R. H. Brandenberger. Searching for Cosmic Strings in New Observational Windows. *ArXiv e-prints*, January 2013, 1301.2856.

[5] Robert H Brandenberger. Topological defects and structure formation. *International Journal of Modern Physics A*, 9(13):2117–2189, 1994.

[6] Cora Dvorkin, Mark Wyman, and Wayne Hu. Cosmic string constraints from WMAP and the South Pole Telescope data. *Phys. Rev. D*, 84:123519, Dec 2011.

[7] Planck Collaboration, P. A. R. Ade, N. Aghanim, C. Armitage-Caplan, M. Arnaud, M. Ashdown, F. Atrio-Barandela, J. Aumont, C. Baccigalupi, A. J. Banday, and et al. Planck 2013 results. XXV. Searches for cosmic strings and other topological defects. *ArXiv e-prints*, March 2013, 1303.5085.

[8] Levon Pogosian, S.-H. Henry Tye, Ira Wasserman, and Mark Wyman. Observational constraints on cosmic string production during brane inflation. *Phys. Rev. D*, 68:023506, Jul 2003.

[9] Mark Wyman, Levon Pogosian, and Ira Wasserman. Bounds on cosmic strings from WMAP and SDSS. *Phys. Rev. D*, 72:023513, Jul 2005.

[10] Aurélien A Fraisse. Limits on defects formation and hybrid inflationary models with three-year WMAP observations. *Journal of Cosmology and Astroparticle Physics*, 2007(03):008.

[11] Richard A Battye, Björn Garbrecht, Adam Moss, and Horace Stoica. Constraints on brane inflation and cosmic strings. *Journal of Cosmology and Astroparticle Physics*, 2008(01):020.

[12] Neil Bevis, Mark Hindmarsh, Martin Kunz, and Jon Urrestilla. CMB power spectrum contribution from cosmic strings using field-evolution simulations of the abelian Higgs model. *Phys. Rev. D*, 75:065015, Mar 2007.

[13] Neil Bevis, Mark Hindmarsh, Martin Kunz, and Jon Urrestilla. Fitting cosmic microwave background data with cosmic strings and inflation. *Phys. Rev. Lett.*, 100:021301, Jan 2008.

[14] Richard Battye and Adam Moss. Updated constraints on the cosmic string tension. *Phys. Rev. D*, 82:023521, Jul 2010.

[15] Robert H. Brandenberger, Rebecca J. Danos, Oscar F. Hernández, and Gilbert P. Holder. The 21 cm signature of cosmic string wakes. *Journal of Cosmology and Astroparticle Physics*, 2010(12):028.

[16] Rishi Khatri and Benjamin D. Wandelt. Cosmic (super)string constraints from 21 cm radiation. *Phys. Rev. Lett.*, 100:091302, Mar 2008.

[17] Aaron Berndsen, Levon Pogosian, and Mark Wyman. Correlations between 21-cm radiation and the cosmic microwave background from active sources. *Monthly Notices of the Royal Astronomical Society*, 407(2). ISSN 1365-2966.

[18] J. J. McMahon, K. A. Aird, B. A. Benson, L. E. Bleem, J. Britton, J. E. Carlstrom, C. L. Chang, H. S. Cho, T. de Haan, T. M. Crawford, A. T. Crites, A. Datesman, M. A. Dobbs, W. Everett, N. W. Halverson, G. P. Holder, W. L. Holzapfel, D. Hrubes, K. D. Irwin, M. Joy, R. Keisler, T. M. Lanting, A. T. Lee, E. M. Leitch, A. Loehr, M. Lueker, J. Mehl, S. S. Meyer, J. J. Mohr, T. E. Montroy, M. D. Niemack, C. C. Ngeow, V. Novosad, S. Padin, T. Plagge, C. Pryke, C. Reichardt, J. E. Ruhl, K. K. Schaffer, L. Shaw, E. Shirokoff, H. G. Spieler, B. Stadler, A. A. Stark, Z. Staniszewski, K. Vanderlinde, J. D. Vieira, G. Wang, R. Williamson, V. Yefremenko, K. W. Yoon, O. Zhan, and A. Zenteno. SPTpol: an instrument for CMB polarization. *AIP Conference Proceedings*, 1185(1): 511–514, 2009.

[19] D. Baumann, M. G. Jackson, P. Adshead, A. Amblard, A. Ashoorioon, N. Bartolo, R. Bean, M. Beltrán, F. de Bernardis, S. Bird, X. Chen, D. J. H. Chung, L. Colombo, A. Cooray, P. Creminelli, S. Dodelson, J. Dunkley, C. Dvorkin, R. Easther, F. Finelli, R. Flauger, M. P. Hertzberg, K. Jones-Smith, S. Kachru, K. Kadota, J. Khoury, W. H. Kinney, E. Komatsu, L. M. Krauss, J. Lesgourgues, A. Liddle, M. Liguori, E. Lim, A. Linde, S. Matarrese, H. Mathur, L. McAllister, A. Melchiorri, A. Nicolis, L. Pagano, H. V. Peiris, M. Peloso, L. Pogosian, E. Pierpaoli, A. Riotto, U. Seljak, L. Senatore, S. Shandera, E. Silverstein, T. Smith, P. Vaudrevange, L. Verde, B. Wandelt, D. Wands, S. Watson, M. Wyman, A. Yadav, W. Valkenburg, and M. Zaldarriaga. Probing inflation with

CMB polarization. In *American Institute of Physics Conference Series*, volume 1141 of *American Institute of Physics Conference Series*, 2009.

[20] D. Hanson, S. Hoover, A. Crites, P.A.R. Ade, K.A. Aird, et al. Detection of B-mode Polarization in the Cosmic Microwave Background with Data from the South Pole Telescope. *ArXiv e-prints*, 2013, 1307.5830.

[21] Rebecca J. Danos, Robert H. Brandenberger, and Gil Holder. A Signature of Cosmic Strings Wakes in the CMB Polarization. *Phys.Rev.D*, D82: 023513, 2010.

[22] A. Vilenkin and E.P.S. Shellard. *Cosmic Strings and Other Topological Defects*. Cambridge Monographs on Mathematical Physics. Cambridge University Press, 2000. ISBN 9780521654760.

[23] T.W.B. Kibble. Topology of cosmic domains and strings. *Journal of Physics A: Mathematical and General*, 9(8):1387.

[24] Wayne Hu and Martin White. A CMB polarization primer. *New Astronomy*, 2(4):323 – 344, 1997. ISSN 1384-1076.

[25] S. Chandrasekhar. *Radiative Transfer*. Dover Books on Intermediate and Advanced Mathematics. DOVER PUBN Incorporated, 1960. ISBN 9780486605906.

[26] Paolo Cabella and Marc Kamionkowski. Theory of cosmic microwave background polarization. *ArXiv e-prints*, 2004, astro-ph/0403392.

[27] J.D. Jackson. *Classical Electrodynamics*. ISBN 9780471309321.

[28] Matias Zaldarriaga and Uroš Seljak. An all sky analysis of polarization in the microwave background. *Phys.Rev.D*, D55:1830–1840, 1997.

[29] Marc Kamionkowski, Arthur Kosowsky, and Albert Stebbins. Statistics of cosmic microwave background polarization. *Phys.Rev.D*, D55:7368–7388, 1997.

[30] Kendrick M. Smith and Matias Zaldarriaga. General solution to the *E*-*B* mixing problem. *Phys. Rev. D*, 76:043001, Aug 2007.

[31] Emory F. Bunn, Matias Zaldarriaga, Max Tegmark, and Angelica de Oliveira-Costa. *E/B* decomposition of finite pixelized CMB maps. *Phys. Rev. D*, 67:023501, Jan 2003.

[32] J. N. Goldberg, A. J. Macfarlane, E. T. Newman, F. Rohrlich, and E. C. G. Sudarshan. Spin-s spherical harmonics and ð. *Journal of Mathematical Physics*, 8(11):2155–2161, 1967.

[33] Manoj Kaplinghat, Mike Chu, Zoltán Haiman, Gilbert P. Holder, Lloyd Knox, and Constantinos Skordis. Probing the reionization history of the universe using the cosmic microwave background polarization. *The Astrophysical Journal*, 583(1):24.

[34] Wayne Hu. Weak lensing of the CMB: A harmonic approach. *Phys. Rev. D*, 62:043007, Jul 2000.

[35] T.W.B. Kibble. Evolution of a system of cosmic strings. *Nuclear Physics B*, 252(0):227 – 244, 1985. ISSN 0550-3213.

[36] Alexei A. Starobinsky. Relict Gravitation Radiation Spectrum and Initial State of the Universe. (In Russian). *JETP Lett.*, 30:682–685, 1979.

[37] B. Allen. Stochastic gravity-wave background in inflationary-universe models. *Phys. Rev. D*, 37:2078–2085, Apr 1988.

[38] A. G. Polnarev. Polarization and Anisotropy Induced in the Microwave Background by Cosmological Gravitational Waves. *Soviet Astronomy*, 29: 607–613, December 1985.

[39] Matias Zaldarriaga and Uroš Seljak. Gravitational lensing effect on cosmic microwave background polarization. *Phys. Rev. D*, 58:023003, Jun 1998.